Solar Energy
And Sustainable Development
Refereed, biannual scientific journal issued by:
The Libyan Center for Solar Energy Research and Studies

Modular Open Source Solar Photovoltaic-Powered DC Nanogrids with Efficient Energy Management System

Md Motakabbir Rahman[1*], Joshua M. Pearce[2].

[1]Department of Electrical & Computer Engineering, Western University, London, ON, Canada.

[2]Ivey Business School, Western University, London, ON, Canada.

E-*mail:* mrahm339@uwo.ca , joshua.pearce@uwo.ca .

ARTICALE INFO.

Article history:
Received 18 Jan 2024
Received in revised form 22 Jan 2024
Accepted 23 Feb 2024
Available online 30 February 2024

KEYWORDS

Distributed Generation; Energy Management System; DC Nanogrid; Photovoltaic; Solar energy; Open Source.

ABSTRACT

Initially the concept of a DC nanogrid was focused on supplying power to individual homes. Techno-economic advances in photovoltaic (PV) technology have enabled solar PV stand-alone nanogrids to power individual devices using device-specific architectures. To reduce costs and increase accessibility for a wider range of people, a modular open-source system is needed to cover all applications at once. This article introduces a modular PV-powered nanogrid system, consisting of a do it yourself (DIY) PV system with batteries to allow for off-grid power. The resultant open-source modular DC nanogrid can deliver DC power to loads of different voltage levels, which is possible because of the efficient and parametric energy management system (EMS) that selects modes of operation for the grid based on DC bus voltage and state of charge of batteries. Simulation results verify the coordination between the EMS and the PV-battery system under varying PV power generation and load conditions. This EMS has potential to enable easy personalization of a vast area of applications and expand appropriate technology for isolated communities. A thorough stability analysis has been conducted, leading to the development of an LQR (Linear Quadratic Regulator) controller as a replacement for the conventional PI (Proportional - Integral) controllers for better transient stability of the system.

NOMENCLATURE:

SoC	State of charge.	J	cost function.
K_p	Proportional gain.	Q	state weighting matrix.
K_i	Integral gain.	R	control weighting matrix.
Z_{ocl}	Closed loop output impedance.	K	LQR gain matrix.
Z_{icl}	closed loop input impedance.	P	Unique positive definite solution of the algebraic Riccati equation (ARE).
Z_{bus}	Total bus impedance.		

*Corresponding author.

DOI: https://doi.org/10.51646/jsesd.v13i1.169

منظومات خلايا شمسية مفتوحة المصدر مدمجة مع شبكات نانونية ونظام إدارة فعال

متكبر رحمن*[1]، جوشا بييرس[2].

ملخص: بداية ركز مفهوم الشبكة النانوية للتيار المستمر (DC) على تزويد المنازل الفردية بالطاقة. وقد مكنت التطورات في مجال التكنولوجيا الكهروضوئية (PV) من تشغيل الأجهزة الفردية باستخدام بنى محددة للجهاز نفسه وباستقلال تام بواسطة الطاقة الشمسية. لتقليل التكاليف وزيادة إمكانية الوصول إلى مجموعة أوسع من الأشخاص، نحتاج إلى نظام مفتوح المصدر ومعياري لتغطية جميع التطبيقات في وقت واحد. يقدم هذا المقال نظامًا نموذجيًا للشبكة النانوية المدعومة بالطاقة الكهروضوئية (PV)، يتكون من نظام «افعلها بنفسك» (DIY) لألواح الخلايا الشمسية مع بطاريات للسماح بالطاقة المستقلة خارج الشبكة التقليدية. يمكن للشبكة النانوية المعيارية ومفتوحة المصدر أن توفر طاقة التيار المستمر (DC) لمختلف مستويات الجهد، وذلك بفضل نظام إدارة الطاقة (EMS) الفعال والذي يختار أوضاع التشغيل للشبكة بناءً على جهد ناقل التيار المستمر (DC) وحالة الشحن في البطاريات. وتؤكد نتائج المحاكاة التنسيق بين نظام إدارة الطاقة (EMS) ونظام البطاريات في ظل ظروف توليد الطاقة الكهروضوئية المتغيرة. يتمتع نظام إدارة الطاقة هذا بإمكانية تمكين التخصيص السهل لمجموعة واسعة من التطبيقات وتوسيع نطاق التكنولوجيا المناسبة للمجتمعات المعزولة. تم إجراء تحليل شامل للاستقرار، مما أدى إلى تطوير وحدة تحكم LQR (منظم تربيعي خطي) كبديل لوحدات التحكم التقليدية PI (التناسبية-التكاملية) لتحسين الاستقرار المؤقت للنظام.

1. INTRODUCTION

A The United Nations has stressed the critical importance of modern energy services access through its Sustainable Development Goal (SDG) 7, which seeks to provide access to affordable, reliable, and sustainable modern energy for all people on earth [1]. The world has made some progress on this front, as the number of people without access to electricity declined from 1.2 billion in 2010 to 759 million in 2019 [2]. These numbers, however, can be misleading as Ayaburi et al., estimate that 3.5 billion people lack "reasonably reliable" access to electricity services [3]. Extending the electric grid is costly [4],[5] and even providing full power with PV and backup to a building can be cost prohibitive despite the clear benefits that it brings [6]. Recent decreases in PV costs [7], [8] offer economically viable power for a range of contexts [9], [10], but high initial investment requirements (particularly for electrical storage that still must decrease for widespread adoption [11]) and technical complexity created barriers to adoption for most consumers. The potential for providing device specific power is a way that can expand reasonably reliable electricity services to billions of people.

Although the initial idea of the nano grid was for supplying power to individual homes [12], with technical and economic advances in solar photovoltaic (PV) technology, stand-alone nanogrid is also used to power individual devices. For example, the on-site solar-powered LED street light project has been designed with PV modules mounted on the top of a pole, with batteries and controllers equipped in a box [13], [14]. Solar-powered electric vehicles (EV) chargers with distinguished architectures have been developed [15], [16]. Solar PV and solar thermal collector-based complete water desalination systems [17], and solar-powered air conditioning, refrigeration, and water cooling [18], [19] have been proposed. Similarly, solar irrigation systems have been designed to supply PV-generated power to single-phase motor/pump [20], [21]. Some similar developments are solar-powered cellular base stations [22], and solar-powered extruders [23] and 3-D printers [24], [25]. These single-device solutions introduced new architectures for each device, rather than a single modular parametric solution that could work for all devices. Consequently, they were unable to leverage the scale of PV production, resulting in higher costs. Furthermore, these examples suggest that most of these loads or devices operate on DC, but their PV solutions involve unnecessary conversion from DC to AC and then back from AC to DC. To reduce costs and increase accessibility for a wider range of people, a modular open-source system is needed to cover all applications at once.

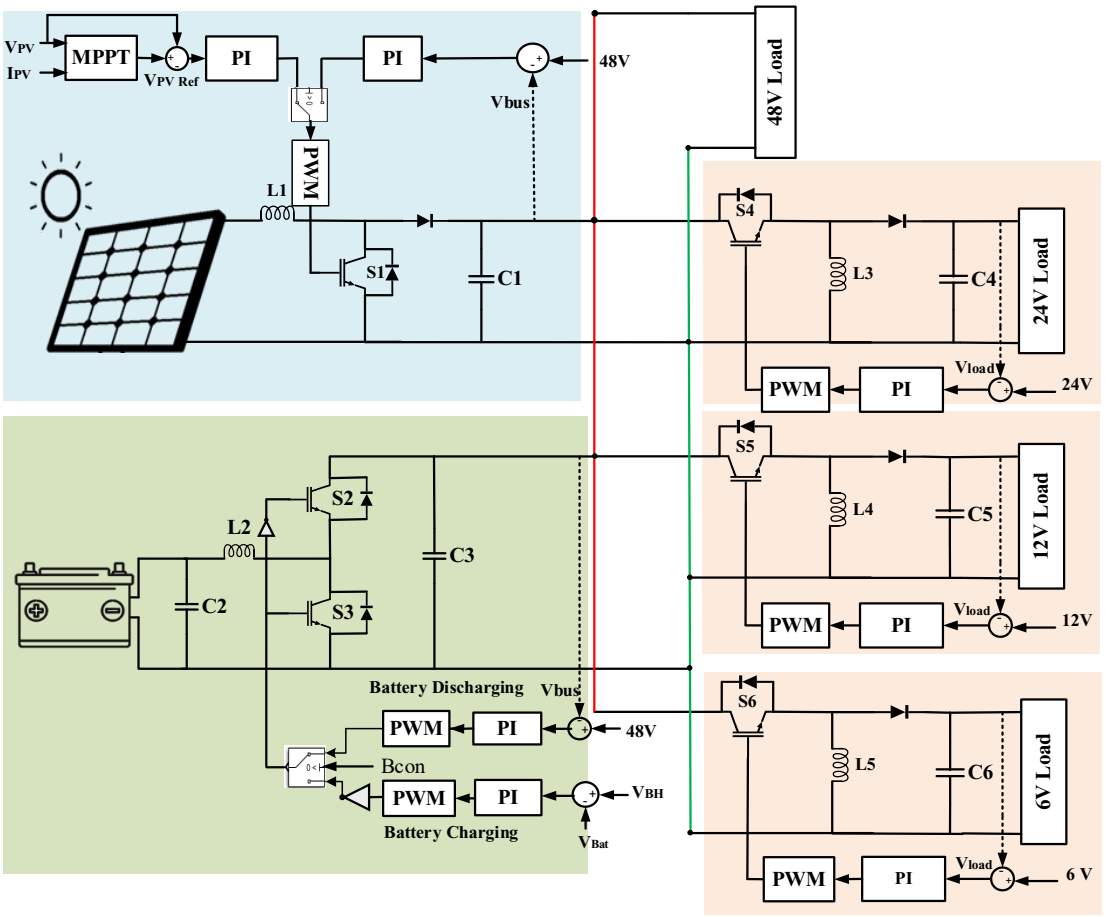

Fig. 1. Architecture of DC nanogrid.

To do this, this article introduces a modular PV-powered nanogrid system [26] with batteries to efficiently deliver DC power to loads operating at various voltage levels . It is licensed open source under GNU GPLv3 and CERN OHL-S v2. The novelty of this work is the energy management system (EMS), which employs parametric controls and selects optimal operating modes for the grid based on the DC bus voltage and battery state of charge (SoC). This setup enables the PV converter, bidirectional battery charging converter, and load converter to operate independently, following commands issued by the central EMS. These units will be interconnected in a modular fashion to a common DC bus, enhancing the overall robustness and flexibility of the solution. Additionally, this arrangement can facilitate the implementation of various charging and maximum power point tracking (MPPT) algorithms easily. This open-source EMS design can serve as a versatile and customizable solution for both current and future solar-powered individual devices. Additionally, a comprehensive stability analysis has been conducted to assess the system's stability. In addition, an LQR controller has been designed to enhance system stability and performance.

The remaining sections are structured as follows: Section 2 presents a concise elucidation of the configuration and EMS of the DC nano grid. Section 3 outlines the design procedure of the controllers and their specifications. Section 4 encompasses the time domain simulation for three distinct scenarios. Section 5 provides comprehensive stability analysis of the bus voltage in the presence of disturbances utilizing impedance scanning and Fast Fourier Transform (FFT) analysis. Section 6 demonstrates the implementation of an advanced Linear Quadratic Regulator (LQR) controller to mitigate oscillations on the DC bus. Finally, Section 7 summarizes major

contributions, and outlines future research plans.

2. METHODS

A. System Architecture:

In the nanogrid architecture (Fig. 1), a 2kW boost converter is used to interface the PV system with the DC bus. On the other side, a bidirectional buck-boost converter of 5kW and three buck converters (total 1.6kW) connect respectively a lithium-ion (li-ion) battery and loads of different voltage levels to the grid. [27], [28].

In choosing the appropriate DC bus voltage for DC nanogrid, some consideration has been made to ensure user safety, efficiency, and cost saving. Among different low voltage levels ranging from 12V to 100V, 48V voltage level is found to be the best choice for the nanogrid in terms of cost and performance [29]. The nanogrid is also modelled in such a way, that the generation can easily be scaled up by connecting PV modules and their interface converters with the bus. Similarly, additional batteries can be introduced with a bidirectional converter to support any expansion of loads or storage requirements. The centralized control by the energy management system (EMS) can accommodate any variation in DC load and weather conditions. Thus, this paper introduces the modular and adaptive architecture of a PV system with free and open source software [30]. However, it is crucial to ensure that the cumulative ratings of the solar panels, batteries, and loads do not surpass the originally specified power limits of the nano-grid. The source code for this project is released under GNU GPL v3[31]. All simulations were performed in Matlab/Simulink. All cases evaluated in this study are included in Simulink file format in the Open Science Framework repository. Open source development allows for rapid innovation [32], [33] and has been called for in the PV sector [34]. Additionally, the nanogrid variants can be used to power specific devices and solar powering of open source appropriate technology (OSAT) [35].

B. Energy Management System (EMS):

Previously, the power management systems used in nanogrids operate based on the battery voltage [36], while the DC bus voltage is used as an information carrier for mode selection [37], [38]. Other PV and battery parameters such as PV output power, SoC and power limit of the battery, DC loads, and the load demands are also used by the power management systems to decide the operation modes of the system [39]. In this EMS, decisions are made based on DC bus voltage and SoC of battery.

Usually, a DC nanogrid has three different operation modes: 1) power surplus, 2) deficit and 3) battery isolation, based on the instructions given by the EMS [40]. In addition, the EMS coordinately controls [41] all the interface controllers in a centralized manner by providing three different output signals: 1) battery charging/discharging signal, 2) battery isolation signal and 3) PV converter control signal. The upper limit of bus voltage for the surplus mode is selected to be 48+10% (52.8V) and the lower limit for deficit mode is 48-10% (43.2V). Finally, the decision on idle mode (isolation of battery) is made on the upper and lower limit of SoC of battery [42]. The depth of discharge for battery has been chosen to be 60% [49],[50] and based on that the lower limit of SoC is 35% and upper limit 95% are selected. The EMS generates all control signals based on the algorithm depicted in Fig. 2. The entire system is simulated using SIMULINK, and the EMS algorithm is implemented as a MATLAB function.

3. CONTROLLER DESIGN

A. PV Array Converter & Controller:

PV arrays are connected to a boost converter which operates on two modes: battery connected and battery isolation. In battery isolated mode where PV is radially connected to the DC load

without battery, the bus voltage is regulated by the boost converter. The controller in Fig. 3(a) is designed for this mode and has two closed PI loops. The outer loop regulates the DC bus voltage, and the inner loop maintains the V_{PV} voltage, which minimizes the transients during load change.

Table 1. Controller parameters of boost converter[45].

Parameter	Boost Converter
Max load power	2,000 W
Input voltage V_S	30
Output voltage V_{bus}	48
Inductance (L)	L_1=30 µH
Output capacitor (C_{out})	C_1= 680 µF
Proportional gain (K_p)	0.05
Integral gain (K_i)	7.5

On battery connected mode, the controller in Fig. 3 (b) uses MPPT alongside PI controller to maintain the PV arrays at V_{MPP} to extract the maximum power from the PV array. A perturb and observe MPPT algorithm [46] has been used to allow the PV to supply maximum power under varying load condition and varying environmental conditions. For the source side boost converter, the proportional gain (K_p) and integral gain (K_i) are selected respectively (K_p= 0.05 and K_i=7.5) based on the step response closed loop transfer function of boost converter.

B. Load Converter Controller:

Various loads with different voltage levels, such as 48V, 24V, 12V, and 6V, can be connected to the bus bar. Since the bus voltage remains relatively stable at 48V, loads operating at this voltage can be directly connected. However, for loads with other voltage levels, three buck converters equipped with PI controllers (as shown in Fig. 3(d)) are employed. The EMS is responsible for managing load variations and ensuring the stability of both the bus voltage and the load voltages. To determine the appropriate settings for the load-side buck converters, the proportional gain (K_p) and integral gain (K_i) are carefully selected based on step response of closed loop transfer function of the converters. Detailed parameters for the buck converters can be found in Table 2.

Table 2. Specifications of buck converters[45].

Parameter	24V Buck Converter	12V Buck Converter	6V Buck Converter
Max load power	800 W	600 W	200 W
Input voltage V_S	48	48	48
Output voltage V_0	24	12	6
Duty cycle (d)	50 %	25 %	12.5 %
Inductance (L)	L_3=60 µH	L_4=30 µH	L_5=30 µH
Output capacitor (C_{out})	C_4=220 µF	C_5=560 µF	C_6=820 µF
Proportional gain (K_p)	0.0003	0.001	0.0003
Integral gain (K_i)	7.962	23.47	15.2

C. Energy Storage System (ESS) Controller:

The battery is tied to the DC nanogrid by a bi-directional buck boost converter, which can regulate the power flow in either direction. In the power surplus mode, it acts as a buck

converter and the battery gets charged and as a boost converter in power deficit mode [47]–[49].

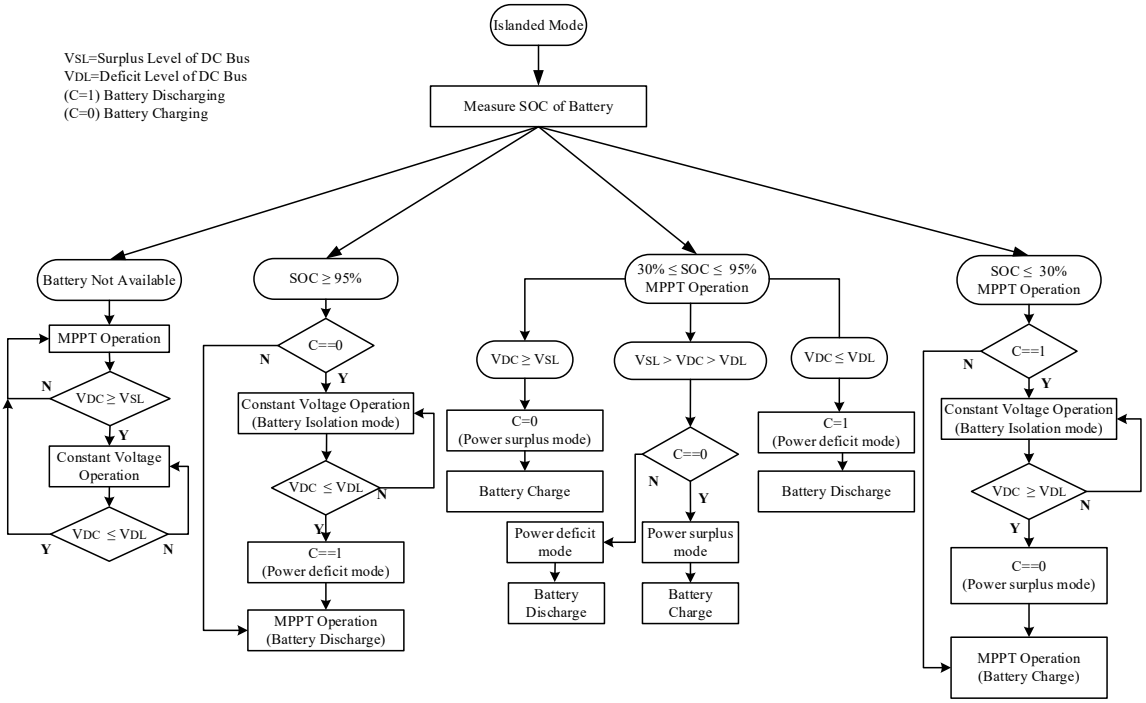

Fig. 2. Flow diagram of Energy Management System.

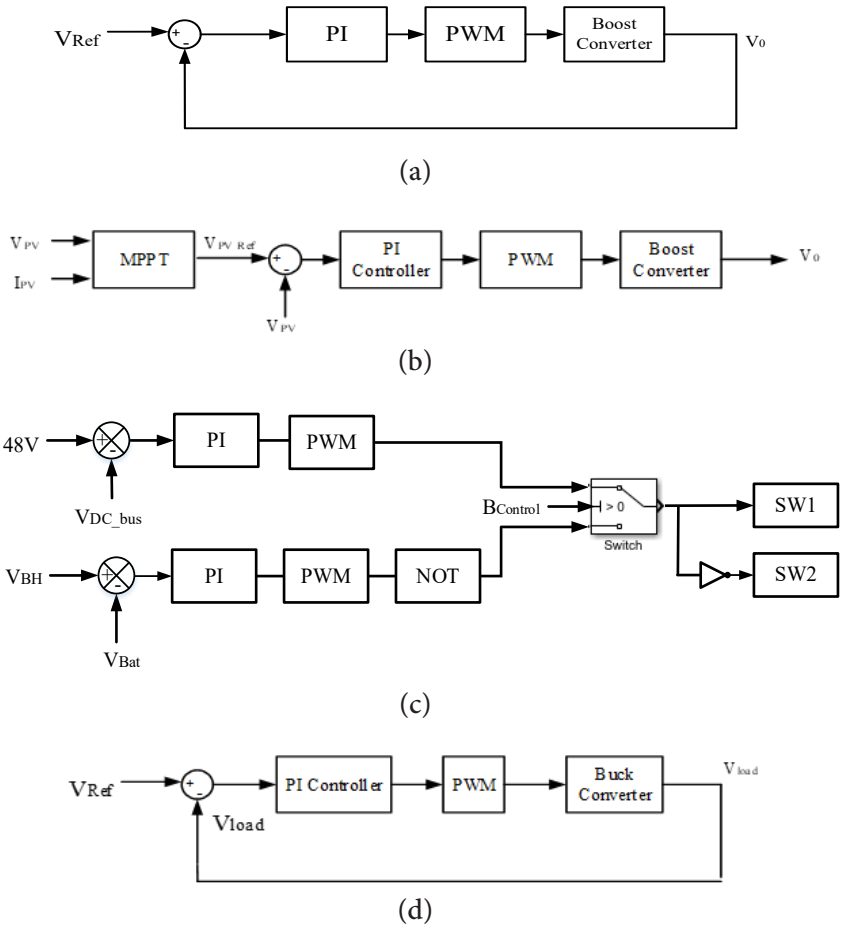

Fig. 3. (a) Controller for isolated PV directly connected with DC load. (b) Controller for battery connected PV array. (c) Battery charge controller. (d) Load voltage controller.

In synchronous buck-boost converters, both switches S_1 and S_2 operate simultaneously, necessitating complementary gate pulses. To illustrate, the inverter symbol is annotated Fig.1. The battery charging controller has two independent PI loops for charging and discharging. When the battery control signal is set to logic 1, it facilitates battery charging and current flows from the DC link to the battery direction. In the event of logic 0, it enables battery discharging and current flow from battery to the DC link. The battery discharged only during power deficit mode which is defined by the bus voltage being below 48V. So, during this the power deficit mode, as depicted in Fig. 3(c), the controller conducts a comparison between the bus voltage and the reference voltage, initiating battery discharge and the bus voltage raised to 48V. Conversely, in the power surplus mode, the controller compares the battery voltage with the battery's maximum charged voltage (V_{BH}) to initiate battery charging. Considering the battery *SoC* is below the 95%, the battery voltage will be lower than the maximum charged voltage and the PI controller will compare them would try to charge the battery up to the maximum battery voltage and as soon as the battery *SoC* become beyond 95%, the battery will be isolated from the system. For the bidirectional converter, the proportional gain (K_p) and integral gain (K_i) along with other parameters are given in Table 3 according to the phase margin (PM) and the gain margin (GM) for the charging mode found respectively (PM= 84^0, GM=21dB) and for discharging mode found (PM=90^0 and GM=25dB), respectively.

Table 3. Specifications of bidirectional buck boost converter.

Parameter	Charging mode	Discharging mode
Max load power	5,000 W	5,000 W
Input voltage	V_{bus} = 48	V_{bat} = 24
Reference voltage	V_{BH} = 27.93	V_{bus} = 48
Inductance (L_2)	L_2= 120 µH	L_2= 120 µH
Capacitor	C_3= 1000 µF	C_3= 1400 µF
Proportional gain (K_p)	0.0005	0.005
Integral gain (K_i)	2.5	3

4. SIMULATION RESULTS

To validate the effectiveness of the EMS and nanogrid, three distinct scenarios have been examined: (1) fluctuation in PV generation, (2) variation in load, and (3) battery isolation triggered by overcharge protection or low state of charge (*SoC*). This section presents time domain simulations of dc bus voltage and power flow for each case. The specifications of PV array and the battery bank under standard test conditions (STC) are given in Table 4.

Table 4. Basic parameters of pv battery system under stc.

Parameters	Values
PV maximum power (P_{PV}^{MPPT})	1532 W
PV maximum power voltage (V_{MPPT})	29.3 V
Battery capacity	200 Ah
Battery fully charged voltage (V_{BH})	27.94 V
Battery nominal voltage	24 V
Battery maximum charging current	20 A
Nominal discharge current	86.96 A

A. Case 1: Variation in PV power generation:

In this case, the nanogrid operates under varying irradiance conditions, leading to fluctuations in PV generation. Based on the simulation results depicted in Fig. 4, initially the solar irradiation is set at 1,000W/m^2, with an ambient temperature of 300K and a maximum PV output of 1,532W. Consequently, all DC loads listed in Table 5 are supplied by the PV source, while any excess power is directed towards charging the battery.

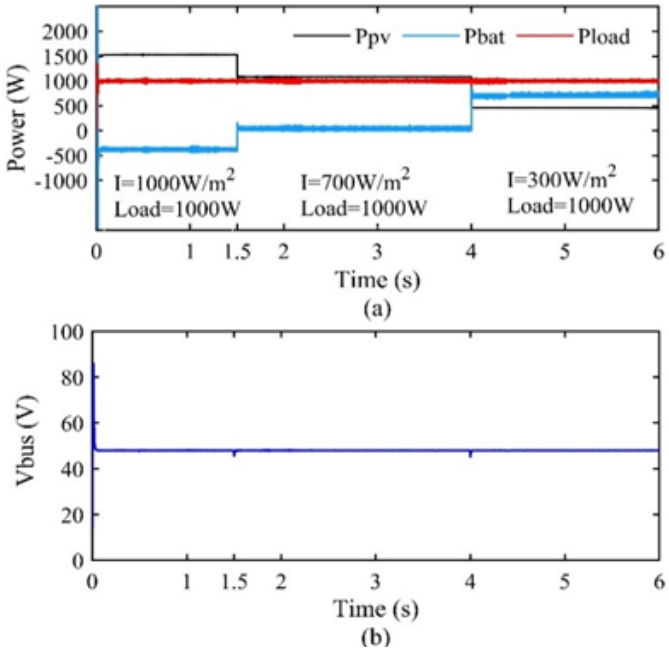

Fig. 4. Case 1: PV power variation (a) power flows (PV, ESS and DC load) and (b) DC bus voltage.

At the 1.5 sec, there was a transition in irradiance to 700 W/m^2, the PV output decreased to 1083 W, yet the system continued to operate with a surplus of power. During this period, the battery was charged with an excess power of 83W. Subsequently, at the 3.5s, the irradiance was further reduced to 300 W/m^2. The PV power output decreased to 462 W, causing the system to enter a power deficit mode. But the dc bus voltage remained steady at 48V throughout the simulation period.

Table 5. Constant dc load for case 1.

Voltage level	Load
24 V load	576 W
12 V load	344 W
6 V load	80 W
Total	1000 W

B. Case 2: Variation in load:

Based on the simulation results at Fig. 5, the DC bus voltage exhibits stability even as the DC loads fluctuate in accordance with Table 6. Throughout the entire simulation, the power generated by the PV source remains constant at 775W, corresponding to an irradiance level of 500 W/m^2. Initially, the system operates in a power deficit mode since the load exceeds the PV power. Subsequently, a slight reduction in the loads to 800W at the 1.5sec leads to a decrease in the power supplied by the battery. The system, however, continues to remain in a power deficit mode. Finally, at the 4sec, a significant decrease in the load to 400W shifts the system into power surplus mode, allowing the system to charge the battery with 375W.

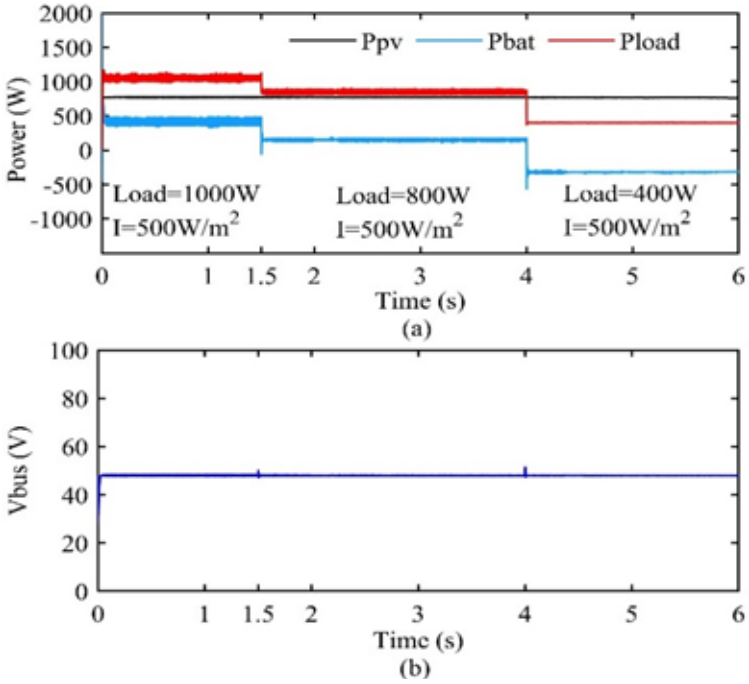

Fig. 5. Case 2: PV power variation (a) power flows (PV, ESS and DC load) and (b) DC bus voltage.

Table 6. Variable dc load for case 2.

Voltage level	0-1.5	1.5-34	34-46
24 V load	576 W	288 W	192 W
12 V load	144 W	232 W	72 W
6 V load	280 W	280 W	136 W
Total	1000 W	800 W	400 W

C. Case 3: Isolation of Battery:

During typical operational conditions, when the battery's state of charge (*SoC*) remains within the prescribed lower (35%) and upper (95%) limits, the PV array diligently tracks the maximum power point voltage (V_{MPP}) as provided by the MPPT algorithm.

In scenarios characterized by power deficit mode when *SoC* is below 35% or power surplus mode when *SoC* is above 95%, the EMS takes measures to isolate the battery from the system. In these instances, the PV module acts as an independent power source, ensuring a continuous supply to the loads, while simultaneously maintaining the bus voltage at 48V.

To confirm the isolation condition, the *SoC* of the battery is set at 94.995% and the system is operating in a power surplus mode ($P_{pv} > P_{load}$).

The study considers the parameters outlined in Table 7. Fig. 6(c) illustrates that the battery becomes isolated from the system as soon as its SoC reaches 95% (at 2.4 seconds). The battery remains in isolation until the system transitions back into power deficit mode ($P_{pv} < P_{load}$) at 4 seconds, triggered by a change in irradiance to 300W/m^2. Subsequently, the battery initiates discharge.

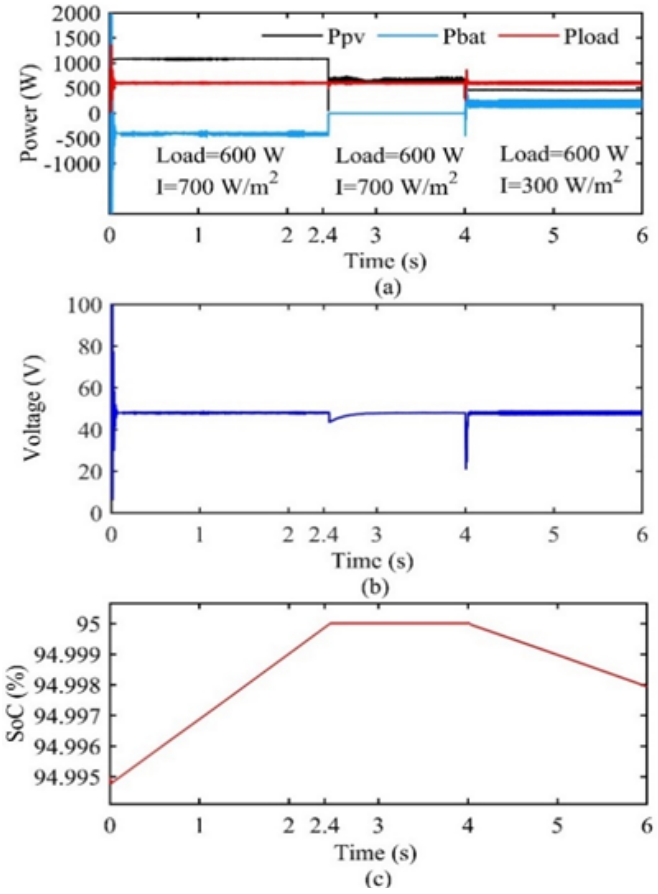

Fig. 6. Case 3: Isolation of battery (a) power flows (PV, ESS and DC load), (b) DC bus voltage and (c) *SoC* of battery.

Table 7. Parameters for case 3.

Power mode	**0-1.4**	**1.4-4**	**4-6**
Irradiance	700 W	700 W	300 W
P_{PV}	1083 W	600 W	462 W
DC *load*	600 W	600 W	600 W
P_{BAT}	-483 W	-	138 W

The time domain simulation effectively demonstrates that the system and EMS consistently maintain the optimal power flow among the PV source, battery, and load across various scenarios. Furthermore, the bus voltage is maintained at 48V. During load and irradiance variations, however, notable fluctuations are observed in the bus voltage, primarily due to the interactions between converters and their resonant frequencies. Hence, in the subsequent section, a comprehensive stability analysis will be conducted to discern the underlying causes and develop alternative controllers to mitigate these transients effectively.

5. STABILITY ANALYSIS

In the time domain simulation, fluctuations in the bus voltage were noted when alterations occurred in the load and irradiance. In this section both impedance scanning and FFT analysis will be utilized to evaluate the stability of the DC nanogrid system and ascertain the reasons behind these voltage fluctuations.

A. Impedance Analysis:

The impedance scanning has been used extensively with the Nyquist Plot to analyze the small signal stability of interconnected systems [50]. This method serves as a valuable tool for assessing the stability of converter-based interconnected systems, enabling the identification of harmonics originating from both sources and load converters. Moreover, it conducts a comprehensive analysis of the entire system by considering the input-output characteristics (impedance) of each subsystem [51]. To check the stability the whole system is into source side impedance Z_s and load side impedance Z_L. In accordance with Nyquist theory, Small Signal Stability (SSS) can be determined by the ratio of $\frac{Z_S}{Z_L}$. The system is stable if the Nyquist plot of $\frac{Z_S}{Z_L}$ curve does not encircle (-1,0) point in the negative plane [52], [53]. To obstruct the circle and to insure the small signal stability, the source impedance should be much smaller than the load impedance of the converter within all frequency ranges, i.e., $|Z_s| << |Z_L|$ [54].

In the DC nano grid system, the open loop output impedance of the boost converter can be expressed as,

$$Z_{ocl}(s) = \frac{Z_o(S)}{1+T(S)} \qquad \text{.....(1)}$$

Where the open loop output impedance of boost converter and bidirectional converter in (battery discharging mode) is,

$$Z_o = \frac{sLR}{s^2LRC + sL + RD'^2} \qquad \text{.....(2)}$$

Loop gains T(s) of the boost converter with PI controller is,

$$T(s) = \left(K_p + \frac{K_i}{s}\right) \times \frac{V_s}{D'^2} \left(\frac{1 - \frac{sL_2}{RD'^2}}{1 + s^2 \frac{L_2C_3}{D'^2} + s\frac{L_2}{RD'^2}} \right) \text{.....(3)}$$

And since the source converters are connected in parallel so the total impedance can be written as the following:

$$Z_{tsource} = \frac{Z_{ocl1} \times Z_{ocl2}}{Z_{ocl1} + Z_{ocl2}} \qquad \text{.....(4)}$$

On the other side, the closed loop input impedance of the buck converter can be expressed as [55],

$$Z_{icl}(s) = \frac{Z_i(s) \times R_2 \times (1 + T(s))}{R_2 - D^2 \times T(s) \times Z_i(s)} \qquad \text{.....(5)}$$

Where the open loop input impedance of buck converter and buck boost converter in (battery charging mode) is,

$$Z_i = \frac{1}{D^2} \left(\frac{s^2LRC + sL + R}{1 + sRC} \right) \qquad \text{.....(6)}$$

Loop gains T(s) of the buck converter with PI controller is,

$$T(s) = \left(K_p + \frac{K_i}{s}\right) \times V_s \left(\frac{1}{1 + s^2LC + s\frac{L}{R}} \right) \qquad \text{.....(7)}$$

Similarly, the total impedance can be written as,

$$Z_{tload} = \frac{Z_{icl1} \times Z_{icl2} \times Z_{icl3}}{Z_{icl1} \times Z_{icl2} + Z_{icl2} \times Z_{icl3} + Z_{icl3} \times Z_{icl1}} \qquad \text{.....(8)}$$

Eventually the total DC bus impedance can be expressed as,

$$Z_{bus} = \frac{Z_{tsource} \times Z_{tload}}{Z_{tsource} + Z_{tload}} \quad \text{.....(9)}$$

The Nyquist plot of the source-to-load impedance ratio of DC nano grid presented in Fig. 7 demonstrating a significant separation from the (-1,0) point. Consequently, it is evident that the system can be deemed stable.

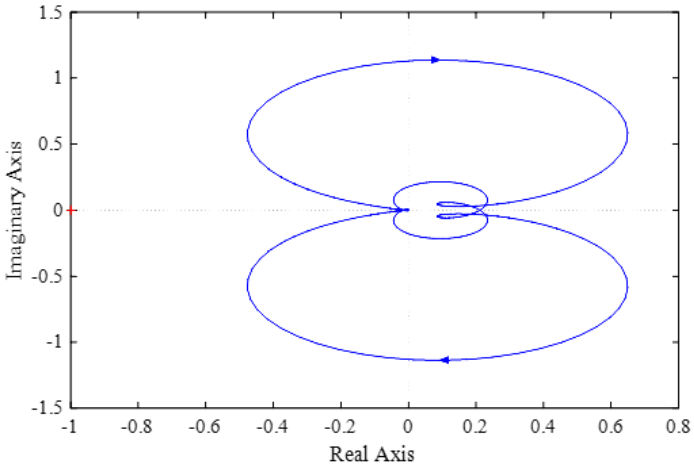

Fig. 7. Nyquist plot of $\frac{Z_S}{Z_L}$.

Moreover, upon examining the Bode plot of both the input and output impedance, it is evident that the magnitude of the source side output impedance consistently remains lower than that of the load side input impedance.

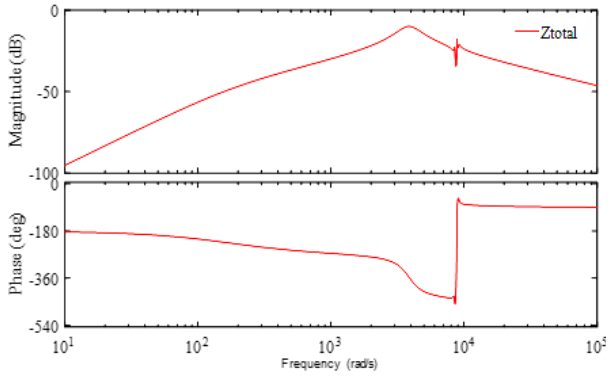

(a)

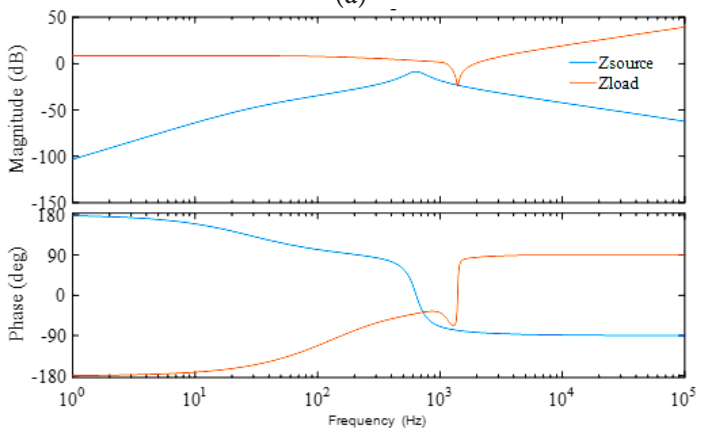

(b)

Fig. 8 (a) Bode plot of source side impedance and load side impedance (b) Bode plot of the total DC bus impedance.

This characteristic ensures the stability of the DC nanogrid across a wide frequency range. Analyzing the frequency response of the overall bus voltage in Fig. 8(b) reveals that the frequency mode responsible for the observed oscillation is 580Hz and 1300 Hz, closely aligning with the resonance frequency of the boost and bidirectional converter. Excluding these resonance peaks, however, results in the overall magnitude of the impedance response remaining within acceptable limits.

B. Fast Fourier Transform (FFT) Analysis:

From impedance analysis it is evident that oscillations are likely attributed to the interaction among the DC converters on the source side, as their resonance frequency is closer to the disturbance frequency range. It is, however, not possible to identify the exact source of disturbance from the impedance scanning. Thus, to identify the exact source of the oscillation, a Fast Fourier Transform (FFT) analysis is conducted [56]. Initially, an AC source with a frequency of 580 Hz and amplitude of 500mV is introduced to the source side of the boost converter. Subsequently, the DC bus voltage undergoes FFT analysis. The results of the FFT analysis indicate that the peak of the oscillation aligns closely with the frequency of the applied AC disturbance, confirming that the source converter is responsible for the oscillation in the DC bus voltage, specifically contributing to the 580 Hz oscillation on the bus.

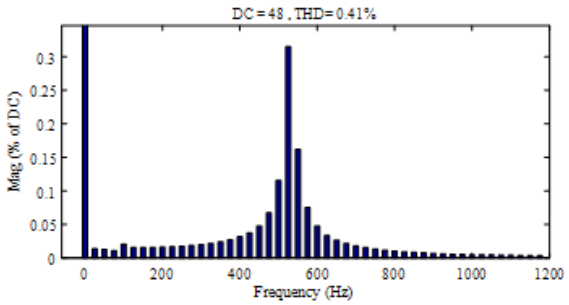

Fig. 9. FFT analysis of the bus voltage under the disturbance on the boost converter's input side.

6. LQR CONTROLLER DESIGN AND PERFORMANCE

As mentioned in the preceding section, both the boost converter and bidirectional converter have been identified as the underlying causes of the transients observed in the bus voltage. To address these oscillations and improve the stability of the DC nanogrid, the application of optimal control techniques is recommended [57]. Various optimal control methods are available, including the Linear Quadratic Regulator (LQR), Linear Quadratic Gaussian (LQG), and Model Predictive Control (MPC). For this particular study, the LQR control scheme will be employed, allowing for the control of the boost converter[58]. This control technique is different from conventional PI controller and requires small signal state space modelling of the converter to design the controller.

A. LQR controller design:

The boost converter can be represented by the following two equations in state space modelling.

$$\dot{x} = Ax + Bu \qquad \text{.....(10)}$$

$$y = Cx + Du \qquad \text{.....(11)}$$

where input and output matrix are considered as,

$$x = \begin{bmatrix} i_L \\ v_o \end{bmatrix} \qquad and \qquad u = \begin{bmatrix} d \end{bmatrix}$$

Using small signal modelling technique and after averaging and linearizing the state equations of the boost converter can be found,

$$\dot{x} = \begin{bmatrix} 0 & -\frac{(1-D_1)}{L} \\ \frac{(1-D_1)}{c} & -\frac{1}{R\times c} \end{bmatrix} x + \begin{bmatrix} \frac{V_{in}}{L\times(1-D_1)} \\ -\frac{V_{in}}{R\times c\times(1-D_1)^2} \end{bmatrix} u \qquad ....(12)$$

$$y = [0 \quad 1]x + [0]u \qquad .....(13)$$

A controller is designed that produces optimal responses of the closed loop system, in the sense of minimizing a performance index or cost function J which can be defined as,

$$J = \int_0^\infty \left(x^T Q x + u^T R u \right) \qquad dt \qquad .....(14)$$

where Q is the state weighting matrix and R is the control weighting matrix. The control signal is defined as,

$$u = -Kx \qquad .....(15)$$

The LQR controller gain matrix K must be determined in such a way that it enhances the performance of the system while minimizing a cost function J. The block diagram of the LQR controller is shown in Fig. 10.

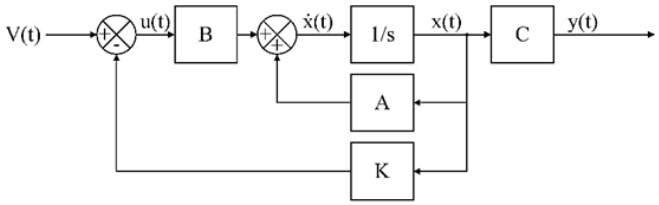

Fig. 10. Block diagram of the LQR controller.

With K being the LQR gain matrix, which is given by,

$$K = R^{-1}B^T P \qquad .....(16)$$

where P is the unique positive definite solution of the algebraic Riccati equation (ARE).

$$A^T P + PA - PBR^{-1}B^T P + Q = 0 \qquad .....(17)$$

By selecting a proper Q and R the LQR gain matrix can be obtained. However, the conventional LQR controller lacks an integral component, and since the boost converter itself does not possess an integrator, it is not possible to achieve a steady-state error of zero solely through state feedback control. To address this limitation, an extended version of the LQR controller is employed, incorporating an integrator. The error between the desired output and the actual output is fed into an integrator, resulting in the creation of a new state variable denoted as $\dot{z}$. This new state variable is then multiplied by the integrator gain, represented as K_i, and subsequently added to the control input as shown in Fig. 11 [59].

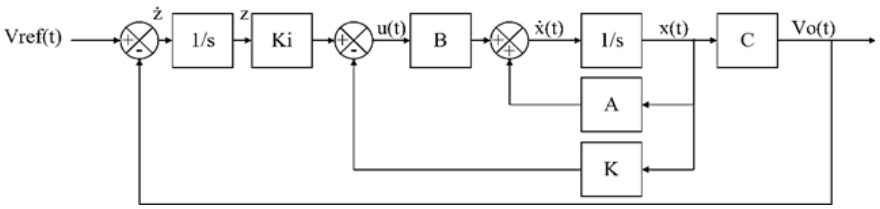

Fig. 11. Block diagram of LQR controller with integral action.

With the inclusion of integral, the control signal (u) becomes,

$$u = K_i z - Kx \qquad and \qquad \dot{z} = V_{ref} - V_o$$

So now the state equation with the integrator becomes,

$$\begin{bmatrix} \dot{x} \\ \dot{z} \end{bmatrix} = A_f \begin{bmatrix} x \\ z \end{bmatrix} + B_f u \qquad .....(18)$$

$$y = C_f \begin{bmatrix} x \\ z \end{bmatrix} \qquad .....(19)$$

Where:

$$A_f = \begin{bmatrix} A - BK & BK_i \\ -C & 0 \end{bmatrix} \quad ,$$

$$B_f = \begin{bmatrix} 0 \\ 0 \\ 1 \end{bmatrix} \quad , \quad and \qquad C_f = \begin{bmatrix} C & 0 \end{bmatrix} \quad .$$

Now the gain matrix can be written as followings,

$$K_d = \begin{bmatrix} K & -K \end{bmatrix} \qquad .....(20)$$

Q and R are selected arbitrarily based on the controller response, and using the MATLAB command the value of K matrix gain and integral gain is determined.

$$Q = \begin{bmatrix} 1 & 1 & 0 \\ 0 & 0.1 & 0 \\ 0 & 0 & 100000 \end{bmatrix}$$

$$R = \begin{bmatrix} 10 \end{bmatrix}$$

$$K = \begin{bmatrix} 0.3190 & 0.0301 \end{bmatrix} \qquad and \qquad K_i = 100.0000$$

B. LQR controller performance:

The new state $\dot{z}$ is found by subtracting the measured output voltage of the boost converter from the reference. And the duty cycle of the boost converter, represented as d, can be determined based on the control input u generated by the LQR controller. The duty cycle is fed into a pulse width modulation (PWM) generator to generate the necessary pulses for the switch. Fig. 12 illustrates a comparison of the response of the boost converter when controlled by both the LQR controller and the PI controller.

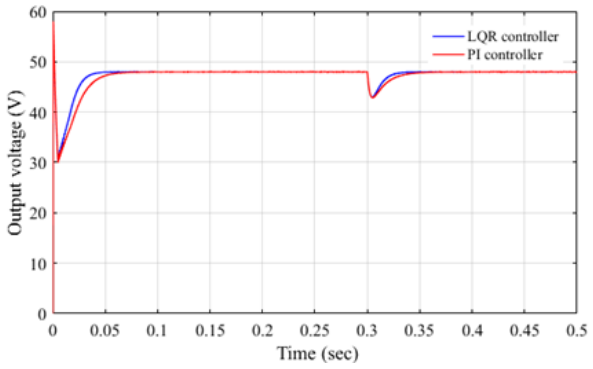

Fig. 12. Output voltage response boost converter of the LQR controller and PI controller.

The results clearly demonstrate that the LQR controller with integral control exhibits superior performance in attaining steady-state conditions at a faster time compared to the PI controller.

C. FFT analysis:

FFT response of the LQR controlled nano grid bus voltage still shows harmonics which has profound peak at 580Hz. However, with the replacement of the PI controller by LQR controller, the occurrence of harmonics is significantly reduced. This reduction is evident in the total harmonic distortion (THD) value, which decreases to 0.24% compared to the earlier value of 0.41% obtained with the PI controller, suggesting that the LQR controller increases the transient stability of the nano grid.

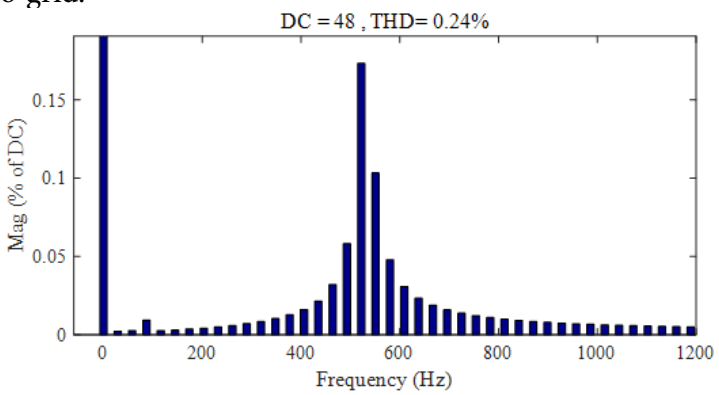

Fig. 13. FFT analysis of the bus voltage under with LQR controller.

7. CONCLUSIONS

This paper presented a modular DC nanogrid which can serve as a flexible solution for current and future solar-powered devices. The key innovation lies in the energy management system (EMS), utilizing parametric controls and selecting optimal operating modes based on the DC bus voltage and battery SoC. The simulation results confirm effective coordination between the EMS and the PV-battery system under diverse conditions. The model facilitates easy integration of new PV panels and loads while maintaining the bus voltage at a stable 48V. Additionally, a comprehensive stability analysis ensures reliable system performance. Moreover, an LQR controller is designed to enhance stability and minimize harmonics, successfully reducing total harmonic distortion (THD) to 0.24%. The nano grid enables a personalized, generic model for various applications, such as off-grid isolated houses, businesses, camps, expedition vehicles, radar stations, and cellular towers. The potential of this open-source solar-powered nano grid extends to re-evaluating electrical technologies for isolated communities where traditional electrical service is unreliable or missing. The DC nano grid holds promise for widespread adoption, enhancing access to sustainable and efficient energy solutions.

Author Contributions: The concept and design of the study were developed by both Rahman and Pearce. Rahman developed the simulations and gathered data. Rahaman and Pearce analyzed the data and collaborated on writing the manuscript. Pearce acquired the funding and provided the materials. After reading the final version of the manuscript, all authors have given their approval.

Funding: This work was supported in part by the Natural Sciences and Engineering Research Council of Canada and the Thompson Endowment.

Data Availability Statement: All data for this article including the simulations profiles are

available on the Open Science Framework: DOI 10.17605/OSF.IO/SV84N.
Acknowledgments: The authors would like to thank K.S. Hayibo for helpful discussions.
Conflicts of Interest: The authors declare that there is no conflict of interest.

REFERENCES

[1] "Take Action for the Sustainable Development Goals - United Nations Sustainable Development." https://www.un.org/sustainabledevelopment/ sustainable-development-goals/ (accessed Nov. 08, 2022).

[2] "Report: Universal Access to Sustainable Energy Will Remain Elusive Without Addressing Inequalities," World Bank. https://www.worldbank. org/en/news/press-release/2021/06/07/report-universal-access-to-sustainable-energy-will-remain-elusive-without-addressing-inequalities (accessed Nov. 08, 2022).

[3] J. Ayaburi, M. Bazilian, J. Kincer, and T. Moss, "Measuring 'Reasonably Reliable' access to electricity services," Electr. J., vol. 33, no. 7, p. 106828, Aug. 2020, doi: 10.1016/j.tej.2020.106828.

[4] S. Szabó, K. Bódis, T. Huld, and M. Moner-Girona, "Energy solutions in rural Africa: mapping electrification costs of distributed solar and diesel generation versus grid extension," Environ. Res. Lett., vol. 6, no. 3, p. 034002, Jul. 2011, doi: 10.1088/1748-9326/6/3/034002.*

[5] D. Palit and K. R. Bandyopadhyay, "Rural electricity access in South Asia: Is grid extension the remedy? A critical review," Renew. Sustain. Energy Rev., vol. 60, pp. 1505–1515, Jul. 2016, doi: 10.1016/j.rser.2016.03.034.

[6] M. Kintner-Meyer, K. Schneider, and R. Pratt, "Impacts assessment of plug-in hybrid vehicles on electric utilities and regional U.S. power grids part 1: technical analysis," Pacific Northwest National Laboratory, Richland, WA, Tech. Rep., 2007.

[7] C. F. Yu, W. G. J. H. M. van Sark, and E. A. Alsema, "Unraveling the photovoltaic technology learning curve by incorporation of input price changes and scale effects," Renew. Sustain. Energy Rev., vol. 15, no. 1, pp. 324–337, Jan. 2011, doi: 10.1016/j.rser.2010.09.001.

[8] A. M. Elshurafa, S. R. Albardi, S. Bigerna, and C. A. Bollino, "Estimating the learning curve of solar PV balance–of–system for over 20 countries: Implications and policy recommendations," J. Clean. Prod., vol. 196, pp. 122–134, Sep. 2018, doi: 10.1016/j.jclepro.2018.06.016.

[9] M. Kamran et al., "Solar Photovoltaic Grid Parity: A Review of Issues, Challenges and Status of Different PV Markets," Int. J. Renew. Energy Res. IJRER, vol. 9, no. 1, Art. no. 1, Mar. 2019.

[10] A. A. Adesanya and J. M. Pearce, "Economic viability of captive off-grid solar photovoltaic and diesel hybrid energy systems for the Nigerian private sector," Renew. Sustain. Energy Rev., vol. 114, p. 109348, Oct. 2019, doi: 10.1016/j.rser.2019.109348.

[11] A. M. Ershad, F. Ueckerdt, R. C. Pietzcker, A. Giannousakis, and G. Luderer, "A further decline in battery storage costs can pave the way for a solar PV-dominated Indian power system," Renew. Sustain. Energy Transit., vol. 1, p. 100006, Aug. 2021, doi: 10.1016/j.rset.2021.100006.

[12] S. C. Joseph, S. Ashok, and P. R. Dhanesh, "Low voltage direct current(LVDC) nanogrid for

home application," in 2017 IEEE Region 10 Symposium (TENSYMP), Jul. 2017, pp. 1–5. doi: 10.1109/TENCONSpring.2017.8069993.

[13] N. M. Kumar, A. K. Singh, and K. V. K. Reddy, "Fossil Fuel to Solar Power: A Sustainable Technical Design for Street Lighting in Fugar City, Nigeria," Procedia Comput. Sci., vol. 93, pp. 956–966, Jan. 2016, doi: 10.1016/j.procs.2016.07.284.

[14] P. Primiceri and P. Visconti, "Solar-powered led-based lighting facilities: an overview on recent technologies and embedded IoT devices to obtain wireless control, energy savings and quick maintenance," vol. 12, no. 1, p. 11, 2017.

[15] M. Dallard, A. Forest, and A. Shabani, "Design of a portable smart connected solar-powered charger for consumer electronics," in 2017 IEEE 30th Canadian Conference on Electrical and Computer Engineering (CCECE), Apr. 2017, pp. 1–4. doi: 10.1109/CCECE.2017.7946781.

[16] A. Verma, B. Singh, A. Chandra, and K. Al-Haddad, "An Implementation of Solar PV Array Based Multifunctional EV Charger," in 2018 IEEE Transportation Electrification Conference and Expo (ITEC), Jun. 2018, pp. 531–536. doi: 10.1109/ITEC.2018.8450191.

[17] M. R. Qtaishat and F. Banat, "Desalination by solar powered membrane distillation systems," Desalination, vol. 308, pp. 186–197, Jan. 2013, doi: 10.1016/j.desal.2012.01.021.

[18] S. McCarney, J. Robertson, J. Arnaud, K. Lorenson, and J. Lloyd, "Using solar-powered refrigeration for vaccine storage where other sources of reliable electricity are inadequate or costly," Vaccine, vol. 31, no. 51, pp. 6050–6057, Dec. 2013, doi: 10.1016/j.vaccine.2013.07.076.

[19] I. Daut, M. Adzrie, M. Irwanto, P. Ibrahim, and M. Fitra, "Solar Powered Air Conditioning System," Energy Procedia, vol. 36, pp. 444–453, Jan. 2013, doi: 10.1016/j.egypro.2013.07.050.

[20] B. Singh, A. K. Mishra, and R. Kumar, "Solar Powered Water Pumping System Employing Switched Reluctance Motor Drive," IEEE Trans. Ind. Appl., vol. 52, no. 5, pp. 3949–3957, Sep. 2016, doi: 10.1109/TIA.2016.2564945.

[21] A. W. Kiprono and A. I. Llario, Solar pumping for water supply: harnessing solar power in humanitarian and development contexts. Warwickshire, UK: Practical Action Publishing Ltd, 2020.

[22] A. Jahid, Md. S. Hossain, Md. K. H. Monju, Md. F. Rahman, and Md. F. Hossain, "Techno-Economic and Energy Efficiency Analysis of Optimal Power Supply Solutions for Green Cellular Base Stations," IEEE Access, vol. 8, pp. 43776–43795, 2020, doi: 10.1109/ACCESS.2020.2973130.

[23] S. Zhong, P. Rakhe, and J. M. Pearce, "Energy Payback Time of a Solar Photovoltaic Powered Waste Plastic Recyclebot System," Recycling, vol. 2, no. 2, Art. no. 2, Jun. 2017, doi: 10.3390/recycling2020010.

[24] D. L. King, A. Babasola, J. Rozario, and J. M. Pearce, "Mobile Open-Source Solar-Powered 3-D Printers for Distributed Manufacturing in Off-Grid Communities," Chall. Sustain., vol. 2, no. 1, Art. no. 1, Oct. 2014, doi: 10.12924/cis2014.02010018.

[25] J. Gwamuri, D. Franco, K. Y. Khan, L. Gauchia, and J. M. Pearce, "High-Efficiency Solar-

Powered 3-D Printers for Sustainable Development," Machines, vol. 4, no. 1, Art. no. 1, Mar. 2016, doi: 10.3390/machines4010003.

[26] L. Grafman and J. M. Pearce, To catch the sun. Humboldt State Press, 2021.

[27] S. Khan and Md. M. Rahman, "Design and Simulation of Solar DC Nano Grid System from Bangladesh Perspective," in 2021 International Conference on Automation, Control and Mechatronics for Industry 4.0 (ACMI), Jul. 2021, pp. 1–6. doi: 10.1109/ACMI53878.2021.9528159.

[28] R. M. Pindoriya, N. M. Pindoriya, and S. Rajendran, "Simulation of DC/DC converter for DC nano-grid integrated with solar PV generation," in 2015 IEEE Innovative Smart Grid Technologies - Asia (ISGT ASIA), Nov. 2015, pp. 1–6. doi: 10.1109/ISGT-Asia.2015.7387065.

[29] S. Moussa, M. J.-B. Ghorbal, and I. Slama-Belkhodja, "Bus voltage level choice for standalone residential DC nanogrid," Sustain. Cities Soc., vol. 46, p. 101431, Apr. 2019, doi: 10.1016/j.scs.2019.101431.

[30] J. M. Pearce and M. M. Rahman, "Modular Open Source Solar Photovoltaic-Powered DC Nanogrids with Efficient Energy Management System," Dec. 2022, Accessed: Dec. 27, 2022. [Online]. Available: https://osf.io/sv84n/

[31] "The GNU General Public License v3.0 - GNU Project - Free Software Foundation." https://www.gnu.org/licenses/gpl-3.0.en.html (accessed Dec. 27, 2022).

[32] J. Arancio, M. Morales Tirado, and J. Pearce, "Equitable Research Capacity Towards the Sustainable Development Goals: The Case for Open Science Hardware," J. Sci. Policy Gov., vol. 21, no. 02, Dec. 2022, doi: 10.38126/JSPG210202.

[33] S. Chopra and S. D. Dexter, : The Promise of Free and Open Source Software. New York: Routledge, 2007. doi: 10.4324/9780203942147.

[34] A. J. Buitenhuis and J. M. Pearce, "Open-source development of solar photovoltaic technology," Energy Sustain. Dev., vol. 16, no. 3, pp. 379–388, Sep. 2012, doi: 10.1016/j.esd.2012.06.006.

[35] J. M. Pearce, "The case for open source appropriate technology," Environ. Dev. Sustain., vol. 14, no. 3, pp. 425–431, Jun. 2012, doi: 10.1007/s10668-012-9337-9.

[36] B. Indu Rani, G. Saravana Ilango, and C. Nagamani, "Control Strategy for Power Flow Management in a PV System Supplying DC Loads," IEEE Trans. Ind. Electron., vol. 60, no. 8, pp. 3185–3194, Aug. 2013, doi: 10.1109/TIE.2012.2203772.

[37] Y. Zhang, H. J. Jia, and L. Guo, "Energy management strategy of islanded microgrid based on power flow control," in 2012 IEEE PES Innovative Smart Grid Technologies (ISGT), Jan. 2012, pp. 1–8. doi: 10.1109/ISGT.2012.6175644.

[38] K. Gowtham, C. V. Sivaramadurai, P. Hariprasath, and B. Indurani, "A Management of power flow for DC Microgrid with Solar and Wind Energy Sources," in 2018 International Conference on Computer Communication and Informatics (ICCCI), Jan. 2018, pp. 1–5. doi: 10.1109/ICCCI.2018.8441324.

[39] Z. Yi, W. Dong, and A. H. Etemadi, "A Unified Control and Power Management Scheme for PV-Battery-Based Hybrid Microgrids for Both Grid-Connected and Islanded Modes," IEEE Trans. Smart Grid, vol. 9, no. 6, pp. 5975–5985, Nov. 2018, doi: 10.1109/TSG.2017.2700332.

[40] L. Xu and D. Chen, "Control and Operation of a DC Microgrid With Variable Generation and Energy Storage," IEEE Trans. Power Deliv., vol. 26, no. 4, pp. 2513–2522, Oct. 2011, doi: 10.1109/TPWRD.2011.2158456.

[41] [41] H. Fan, W. Yu, and S. Xia, "Review of Control Strategies for DC Nano-Grid," Front. Energy Res., vol. 9, 2021, Accessed: Jul. 03, 2022. [Online]. Available:https://www.frontiersin.org/article/10.3389/fenrg.2021.644926

[42] N. Kondrath, "Bidirectional DC-DC converter topologies and control strategies for interfacing energy storage systems in microgrids: An overview," in 2017 IEEE International Conference on Smart Energy Grid Engineering (SEGE), Aug. 2017, pp. 341–345. doi: 10.1109/SEGE.2017.8052822.

[43] M. I. Hlal, V. K. Ramachandaramurthy, A. Sarhan, A. Pouryekta, and U. Subramaniam, "Optimum battery depth of discharge for off-grid solar PV/battery system," J. Energy Storage, vol. 26, p. 100999, Dec. 2019, doi: 10.1016/j.est.2019.100999.

[44] I.-K. Won, D.-Y. Kim, J.-H. Hwang, J.-H. Lee, and C.-Y. Won, "Lifetime management method of Lithium-ion battery for energy storage system," in 2015 18th International Conference on Electrical Machines and Systems (ICEMS), Oct. 2015, pp. 1375–1380. doi: 10.1109/ICEMS.2015.7385253.

[45] N. Mohan, T. M. Undeland, and W. P. Robbins, Power Electronics: Converters, Applications, and Design. John Wiley & Sons, 2003.

[46] F. Liu, Y. Kang, Y. Zhang, and S. Duan, "Comparison of P&O; hill climbing MPPT methods for grid-connected PV converter," in 2008 3rd IEEE Conference on Industrial Electronics and Applications, Jun. 2008, pp. 804–807. doi: 10.1109/ICIEA.2008.4582626.

[47] M. M. Ur Rehman, F. Zhang, R. Zane, and D. Maksimovic, "Control of bidirectional DC/DC converters in reconfigurable, modular battery systems," in 2017 IEEE Applied Power Electronics Conference and Exposition (APEC), Mar. 2017, pp. 1277–1283. doi: 10.1109/APEC.2017.7930860.

[48] R. Li and F. Shi, "Control and Optimization of Residential Photovoltaic Power Generation System with High Efficiency Isolated Bidirectional DC–DC Converter," IEEE Access, vol. 7, pp. 116107–116122, 2019, doi: 10.1109/ACCESS.2019.2935344.

[49] P. Murugesan, P. W. David, P. Murugesan, and P. Periyasamy, "Battery based mismatch reduction technique for partial shaded solar PV system," Energy, vol. 272, p. 127063, Jun. 2023, doi: 10.1016/j.energy.2023.127063.

[50] M. Amin and M. Molinas, "Non-parametric Impedance based Stability and Controller Bandwidth Extraction from Impedance Measurements of HVDC-connected Wind Farms." arXiv, Apr. 16, 2017. doi: 10.48550/arXiv.1704.04800.

[51] M. Amin and M. Molinas, "Small-Signal Stability Assessment of Power Electronics Based Power

Systems: A Discussion of Impedance- and Eigenvalue-Based Methods," IEEE Trans. Ind. Appl., vol. 53, no. 5, pp. 5014–5030, Sep. 2017, doi: 10.1109/TIA.2017.2712692.

[52] M. Habibullah, M. Nadarajah, R. Sharma, and R. Shah, "A Comprehensive Stability Analysis of Multi-Converter-Based DC Microgrids," 2021, pp. 281–314. doi: 10.1201/9781003058472-8.

[53] M. Habibullah, N. Mithulananthan, F. Zare, and R. Sharma, "Impact of Control Systems on Power Quality at Common DC Bus in DC Grid," in 2019 IEEE PES GTD Grand International Conference and Exposition Asia (GTD Asia), Mar. 2019, pp. 411–416. doi: 10.1109/GTDAsia.2019.8715875.

[54] X. Feng, J. Liu, and F. C. Lee, "Impedance specifications for stable DC distributed power systems," IEEE Trans. Power Electron., vol. 17, no. 2, pp. 157–162, Mar. 2002, doi: 10.1109/63.988825.

[55] R. Ahmadi, D. Paschedag, and M. Ferdowsi, "Closed-loop input and output impedances of DC-DC switching converters operating in voltage and current mode control," in IECON 2010 - 36th Annual Conference on IEEE Industrial Electronics Society, Nov. 2010, pp. 2311–2316. doi: 10.1109/IECON.2010.5675123.

[56] M. Habibullah, K. N. Bhumkittipich, N. Mithulananthan, R. Sharma, and F. Zare, "Damping oscillation and removing resonance in a RE based DC microgrids," IEEE Access, vol. 9, pp. 163516–163525, 2021.

[57] M. Habibullah, N. Mithulananthan, F. Zare, and D. S. Alkaran, "Investigation of power oscillation at common DC bus in DC grid," in 2019 IEEE International Conference on Industrial Technology (ICIT), Feb. 2019, pp. 1695–1700. doi: 10.1109/ICIT.2019.8843694.

[58] A. Brahimi, D. Kerdoun, and A. Boumassata, "Boost Converter Control using LQR and P&O Technique for Maximum Power Point Tracking," in 2022 19th International Multi-Conference on Systems, Signals & Devices (SSD), May 2022, pp.1998–2003.doi: 10.1109/SSD54932.2022.9955798.

[59] K. K. Patri and S. Samanta, "State feedback with integral control for boost converter & its microcontroller implementation," in 2018 IEEMA Engineer Infinite Conference (eTechNxT), Mar. 2018, pp. 1–5. doi: 10.1109/ETECHNXT.2018.8385374.